Bioremediation Journal

ISSN: 1088-9868 (Print) 1547-6529 (Online) Journal homepage: https://www.tandfonline.com/loi/bbrm20

Field-scale bioremediation of arsenic-contaminated groundwater using sulfate-reducing bacteria and biogenic pyrite

Ming-Kuo Lee, James A. Saunders, Theodore Wilson, Eric Levitt, Shahrzad Saffari Ghandehari, Prakash Dhakal, James Redwine, Justin Marks, Zeki M. Billor, Brian Miller, Dong Han & Luxin Wang

To cite this article: Ming-Kuo Lee, James A. Saunders, Theodore Wilson, Eric Levitt, Shahrzad Saffari Ghandehari, Prakash Dhakal, James Redwine, Justin Marks, Zeki M. Billor, Brian Miller, Dong Han & Luxin Wang (2019) Field-scale bioremediation of arsenic-contaminated groundwater using sulfate-reducing bacteria and biogenic pyrite, Bioremediation Journal, 23:1, 1-21, DOI: 10.1080/10889868.2018.1516617

To link to this article: https://doi.org/10.1080/10889868.2018.1516617

BIOREMEDIATION JOURNAL
2019, VOL. 23, NO. 1, 1–21
https://doi.org/10.1080/10889868.2018.1516617

Taylor & Francis
Taylor & Francis Group

Field-scale bioremediation of arsenic-contaminated groundwater using sulfate-reducing bacteria and biogenic pyrite

Ming-Kuo Lee[a], James A. Saunders[a], Theodore Wilson[a], Eric Levitt[a], Shahrzad Saffari Ghandehari[a], Prakash Dhakal[a,b], James Redwine[c], Justin Marks[c], Zeki M. Billor[a], Brian Miller[a], Dong Han[d], and Luxin Wang[d]

[a]Department of Geosciences, Auburn University, Auburn, AL, USA; [b]Soil, Water, and Environmental Sciences, University of Arizona, Tucson, AZ, USA; [c]ANCHOR QEA, LLC, Birmingham, AL, USA; [d]Department of Animal Sciences, Auburn University, Auburn, AL, USA

ABSTRACT

This research demonstrates that biogenic pyrite formed by stimulation of indigenous sulfate-reducing bacteria (SRB) in a natural aquifer can remove dissolved arsenic from contaminated groundwater under strongly reducing conditions. SRB metabolism led to the precipitation of biogenic pyrite nanoparticles capable of sorbing and co-precipitating arsenic. The field site is an industrial site where shallow groundwater in an unconfined sandy aquifer is contaminated by arsenic. Therefore, biodegradable organic carbon, ferrous iron, sulfate, and fertilizer were injected into groundwater and SRB metabolism began about 1 week later. Microscopic, X-ray diffraction, X-ray fluorescence, and electron microprobe analyses confirm the bio-mineralization of pyrite and over time, pyrite nanoparticles grew to form well-formed crystals (1–10 μm in diameter) or spherical aggregates that contain 0.05–0.4 wt. % arsenic, indicative of their capacity to sequester arsenic. Consequently, dissolved arsenic decreased from its initial concentration of 0.3–0.5 mg/L to below the regulatory clean-up standard for the site of 0.05 mg/L in three downgradient wells in a matter of weeks after injection. The main sequestration stage, with total arsenic removal rates greater than 90%, lasted for at least 6 months until the arrival and mixing of untreated groundwater from upgradient. Treated groundwater with most active bacterial sulfate reduction became enriched in heavy ^{34}S (range from 2.02 to 4.00 ‰) compared to unaffected well water (0.40–0.61 ‰). One to three orders of magnitude increases in SRB cells were observed in treated wells for at least 2 months after injection. For a full-scale remediation, the injection of solution should start at positions hydrologically upgradient from the major plume and proceed downgradient. If needed, aquifers may be repeatedly amended with biodegradable organic carbon to reestablish the reducing conditions that favor arsenic sequestration.

KEYWORDS
Remediation of metals-contaminated sites

Introduction

The toxic metalloid arsenic (As) is a common minor constituent in pyrite (FeS_2) formed in low-temperature environments including anoxic marine and estuarine sediments (Huerta-Diaz and Morse 1992; Natter et al. 2012; Lee et al. 2013; Neumann et al. 2013), lake sediments (Wilkin and Ford 2006; Couture, Gobeil, and Tessier 2010) and groundwater systems (Saunders, Pritchett, and Cook 1997; Lowers et al. 2007; Saunders et al. 2008; Lee et al. 2005; Saunders et al. 2016) and even Gulf Coast salt dome cap rocks, where biogenic pyrite contains up to 3.5 wt. % arsenic (Saunders et al. 1996). Furthermore, arsenic is also a common constituent in higher temperature pyrite occurrences including hypothermal systems and igneous and metamorphic rocks (Abraitis, Pattrick, and Vaughan 2004; Deditius et al. 2014; Blanchard et al. 2007; Deditius et al. 2008; Saunders et al. 2014; Mango and Ryan 2015; Zouboulis, Kydros, and Matis 1993). Research has shown that pyrite can be effective in sorbing and removing arsenic from water, and has been proposed as a possible water-treatment technique (Zouboulis, Kydros, and Matis 1993; Jingtai and Fyfe 2000; Bulut et al. 2014). Furthermore, a proof-of-concept experiment was successfully completed in a small field-scale bioremediation of

CONTACT Ming-Kuo Lee leeming@auburn.edu Department of Geosciences, Auburn University, Auburn, AL 36849, USA.
Supplemental data for this article can be accessed at https://doi.org/10.1080/10889868.2018.1516617.
Color versions of one or more of the figures in the article can be found online at www.tandfonline.com/bbrm.

heavy metals including Pb, Cd, Cr, and Zn (Lee and Saunders 2003; Saunders et al. 2005). This paper presents results of a field-scale demonstration designed to test the hypothesis that stimulating natural SRB to make biogenic pyrite could be a viable remediation strategy for removing arsenic in groundwater.

The geochemistry and mineralogy of arsenic are generally well established (Lowers et al. 2007; Smedley and Kinniburgh 2002; Nordstrom 2002; Nordstrom and Archer; O'Day et al. 2004), with the possible exception of what are the stable arsenic-bearing solid phases expected in low-temperature environments. Dissolved arsenic occurs in two oxidation states in most natural waters. Under oxidizing conditions, pentavalent arsenate [As(V)] species ($H_2AsO_4^-$, $HAsO_4^{2-}$, and AsO_4^{3-}) are dominant. Under moderately reducing conditions, trivalent arsenite [As(III)] species H_3AsO_3 predominates over a wide range of pH values (Figure 1). Under even more reducing conditions, solid arsenic sulfides or thioarsenite aqueous complexes may become the dominant phases in sulfur-rich environments (Lee et al. 2005; Saunders et al. 2008) (Figure 1). Orpiment (As_2S_3), realgar (AsS), and arsenopyrite (FeAsS) are the most commonly occurring arsenic minerals under reducing hydrothermal conditions in nature, although metal-arsenide minerals do occur rarely. Under highly reducing conditions, As-bearing pyrite appears to control arsenic solubility in reducing environments containing reactive iron and sulfur (Saunders et al. 2008) (see the section "Results and Discussion"). The geochemistry of arsenic has received new interest and research due to the worldwide problem of arsenic contamination (natural and anthropogenic) of potable drinking water supplies (Smedley and Kinniburgh 2002; Nordstrom and Archer 2003; O'Day 2006; Nordstrom et al. 2014; McArthur et al. 2004).

Observations about the relationship between dissolved arsenic and sulfate in groundwater at multiple scales, including local (site-scale) (Keimowitz et al. 2005), USA state-scale (Kirk et al. 2004), and country-scale (McArthur et al. 2004; Ahmed et al. 2004) generally showed an inverse relationship between As and SO_4. This has been interpreted to indicate that biogenic sulfate reduction can remove dissolved arsenic where sulfate is abundant (Rittle, Drever, and Colberg 1995; Keimowitz et al. 2007; Kirk et al. 2010; Onstott et al. 2011; Omoregie et al. 2013; Burton, Johnston, and Kocar 2014; Sun et al. 2016), and some of those researchers proposed that SRB might prove useful in remediating As-contaminated groundwater (Keimowitz et al. 2005; Kirk et al. 2004). Microcosm experiments using sediment from a natural aquifer suggested that SRB activities would not remove arsenic to concentrations lower than the World Health Organization drinking water standard of 0.01 mg/L (Omoregie et al. 2013). The interaction of dissolved arsenic with any of the Fe-sulfide phases is complicated by the fact that H_2S forms stable aqueous complexes with dissolved arsenic (Bostick, Fendorf, and Brown 2005; Couture et al. 2013), which could enhance As solubility under reducing conditions in the absence of appreciable dissolved iron (Keimowitz et al. 2007). This aqueous complexation process was proposed to explain a concurrent increase in both dissolved As and H_2S in an aquifer with low dissolved iron (Wilkin, Wallschlager, and Ford 2003). Adding to the As–Fe–S system natural complexity are reports in the literature of the low-temperature occurrence of As-sulfides such as a realgar, orpiment, and arsenopyrite (O'Day et al. 2004; O'Day 2006; Langner, Mikutta, and Kretzschmar 2012; Langner et al. 2013; DeSisto, Jamieson, and Parsons 2016). More work is needed

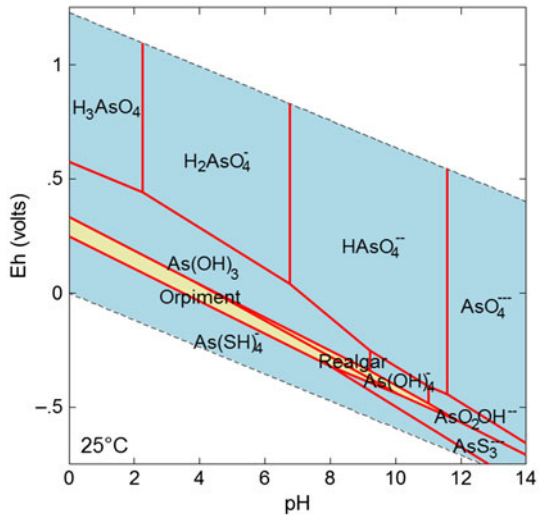

Figure 1. Eh–pH diagram calculated for As–S system at 25 °C and fixed arsenic and sulfate activities of 10^{-6} and 10^{-5}, respectively. The results show the stability field of different arsenic species under different geochemical conditions. Thermodynamic data of various species are shown in Table S1 in Supplementary Material. Plot was constructed using Geochemist's Workbench.

to confirm that amorphous or crystalline As-sulfides can occur in low-pH, As-rich environments such as some industrial sites, acid mine drainage situations, or in oxidized mine tailings. In contrast, the abundant documented occurrences of arsenian pyrite (arsenic-substituted pyrite) in low-temperature, natural environments (Stuckey et al. 2015) indicate that iron-sulfide solids control arsenic solubility under reducing conditions, at least under circum-neutral pH conditions. Saunders et al. 2008, have estimated thermodynamic data for arsenian pyrite and modeling shows that phase indeed is the thermodynamically favored phase.

In this study, sequestration is defined as the adsorption and co-precipitation of dissolved arsenic (thus their removal from groundwater) on sulfide solids formed by biogenic sulfate reduction. Several laboratory studies have evaluated the mechanisms of arsenic removal from solution via the formation of Fe-sulfide solids such as makinawite, troillite, pyrite, and arsenian pyrite (Farquhar et al. 2002; Bostick and Fendorf 2003; Wolthers et al. 2005; Gallegos, Hyun, and Hayes 2007; Gallegos, Hyun, and Hayes 2008; Kim and Batchelor 2009; Jeong, Han, and Hayes 2010; Han et al. 2011; Han et al. 2013; Le Pape et al. 2017). However, debate remains about the removal efficiency as a function of pH, solution chemistry (arsenic concentration, dissolved Fe and sulfide concentration), and types of Fe-sulfide solids (Bostick and Fendorf 2003; Gallegos, Hyun, and Hayes 2007; Gallegos, Hyun, and Hayes 2008; Han et al. 2011; Han et al. 2013; Le Pape et al. 2017; O'Day et al. 2004; Pi et al. 2017). Although some studies showed that high dissolved arsenic concentrations may inhibit iron sulfide transformation and pyrite nucleation (Wolthers, Butler, and Rickard 2007), recent X-ray absorption spectroscopy and fine structure (EXAFS) analysis (Le Pape et al. 2017), clearly demonstrated that arsenian pyrite can crystallize from a solution of dissolved Fe, H_2S, and As at room temperature. Despite strong laboratory evidence for arsenic incorporation into various Fe-sulfide solids, how such sequestration processes operate in natural aquifers and their effectiveness as a viable remediation method remain unclear. One field study (Pi et al. 2017) showed that the formation of iron sulfide by $FeSO_4$ amendment could remove as much as 73% of arsenic in a natural aquifer in less than 1 month. There has been very little research reported on the long-term stability of newly formed iron sulfide phases under changing redox conditions. Onstott et al. (2011) found that oxidation of As-bearing pyrite did not cause arsenic to be released back to the aqueous solutions.

In this study field investigations were conducted to evaluate if SRB could indeed prove useful in remediating arsenic-contaminated groundwater. The necessary permission and permits were obtained to try a field-scale demonstration project at an industrial site in Florida, where our industrial partner requests the company and site name remain anonymous. A herbicide containing arsenic trioxide was used at the site decades earlier, and it eventually contaminated the shallow groundwater. Previously, both a pump-and-treat process and contaminated soil removal were used at the site to diminish and stabilize the arsenic plume in the groundwater. However, site groundwater arsenic concentrations were still elevated (0.3 to >1 mg/L) after the earlier costly remediation approaches. Previous mineralogical and geochemical analyses confirmed very limited precipitation of arsenian pyrite at the site (Starnes 2015). However the contaminated aquifer is under sulfate-limited conditions and thus the natural precipitation of pyrite is not sufficient to remove dissolved arsenic that reaches hundreds of ppb. Thus the aquifer was amended with labile organic carbon and iron sulfate to stimulate metabolism of indigenous SRB. The main objectives of this study were to 1) amend the aquifer with labile organic carbon and iron sulfate to stimulate metabolism of indigenous SRB for bio-mineralization, 2) recover and characterize groundwater and As-sorbed Fe-S solids during different stages of pre- and post-SRB metabolism, 3) conduct long-term monitoring of treated wells to evaluate if there is a finite time interval during which the SRB process is effective and Fe-S biominerals remain stable for arsenic sequestration, and 4) monitor and fingerprint changes in SRB activity in treated groundwater.

Materials and methods

Field procedures

Field injection experiments were conducted at an industrial site in northwest Florida (Figure 2)

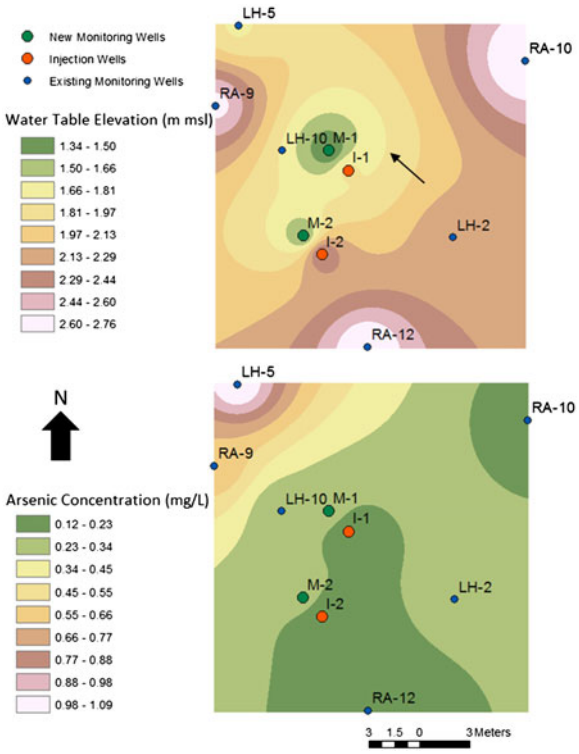

Figure 2. The upper panel shows the pre-injection water table elevations and locations of injection wells (I-1, I-2), new monitoring wells (M-1, M-2), and existing monitoring wells at the site. Arrow shows the general direction of groundwater flow near the injection wells. The lower panel shows interpolated surface showing the distribution of arsenic level (in mg/L) in the aquifer prior to injection.

where shallow groundwater in a surficial aquifer was contaminated by arsenic-bearing herbicide applied at the surface. A number of existing monitoring wells were present at the site (Figure 2), and four new wells were installed for this study in the area of high dissolved arsenic concentration (0.19-0.43 mg/L, Figure 2) using a hollow-stem Auger (HAS)/mud rotary drill rig. New wells include two 10-cm (well casing diameter) injection wells and two 5-cm monitoring wells. Simple volume balance calculations show that the total injection volume of 3000 gallons (11.35 m^3) will displace all pore water residing in the aquifer (with saturation thickness of 6 m and porosity of 0.35) within 1.5 m from injection points. Thus the monitoring wells (M-1 and M-2) were installed approximately 1.5 m downgradient from the injection wells (I-1, I-2; Figure 2) to monitor the effects of biomineralization on arsenic sequestration. The injection wells were screened over the entire thickness of the surficial aquifer above the underlying Jackson Bluff Formation, a regional confining bed (see Supporting Information). During February 15–19, 2016, 2000 gallons of "weak" solution and 1000 gallon of "strong" solution were injected into I-1 and I-2 by gravity feed, using our patented technology (see Supporting Information). Weak solution contains 27.2 kg of molasses, 2.5 kg of ferrous sulfate ($FeSO_4{\cdot}7H_2O$), and 0.9 kg of agricultural-grade fertilizer in 1,000 gallons of water. The amount of ferrous sulfate in the strong solution was two times (5 kg) the amount in the weak solution. The fertilizer contains chloride, which was used as a conservative tracer to track the movement of injectate (with initial chloride concentration of about 200 mg/L) in the aquifer. Groundwater from 10 wells (Figure 2), including two injection wells and two new monitoring wells, were sampled prior to injection to obtain baseline information. After injection, the same ten wells were sampled weekly for the first month, and then monthly thereafter. YSI 556 hand-held multi-parameter probes, connected to an online flow cell, were used in the field to measure water quality parameters including temperature, pH, dissolved oxygen, oxidation–reduction potential (ORP), and electrical conductivity. In YSI 556, the pH and the ORP electrodes are built together as a single probe and the ORP is read relative to the standard SHE, therefore, there is no need for converting the ORP readings to Eh values. Prior to sampling, the wells were purged using a peristaltic pump until all the water quality parameters readings became stabilized. Water samples were filtered using Geotech high-capacity, on-line 0.45 µm filter capsules and then acidified with trace grade HNO_3 (to 3% or 30 g/L nitric acid) for preservation following U.S. EPA standard procedures (Yeskis and Zavala 2015). All water samples were collected in acid-cleaned, high density polyethylene bottles with zero headspace. They were stored in ice-packed coolers (with temperature around 5 °C) immediately after collection. Solid samples precipitated from groundwater were collected using a peristaltic pump from the bottom of the wells where they accumulated by gravity settling. Solid samples were collected from the same ten wells weekly for the first month, and then bimonthly thereafter. Sediment slurry samples

were collected using platinum-cure silicone tubings, then quickly frozen (by dry ice) in a vial with minimum headspaces to preserve the redox state. The same procedure was used for the microbiology samples. The survival and magnitude of individual variability of anaerobic bacteria would not be significantly affected by freezing (Guerin-Danan et al., 1999). Colorimetric techniques were used in the field to measure redox-sensitive elements including dissolved sulfide and ferrous iron. Dissolved sulfide concentration was measured in the field immediately after collection using the Methylene Blue Method in a HACH DR2700 spectrophotometer (USEPA Method 8131). A HACH DR820 colorimeter was used to measure the ferrous iron concentration via 1.10 phenanthroline Method (USEPA Method 8146).

Geochemical analysis of groundwater and biogenic minerals

Major cation and trace element (arsenic and iron) concentrations of groundwater were measured using an Agilent 7900 quadrupole inductively coupled plasma mass spectrometry (ICP-MS) at Auburn University. Anion concentrations were measured using a Dionex 2000 ion chromatograph (IC). The crystalline structure, chemistry, geomorphology, and arsenic contents of the precipitated solids were investigated by several techniques: (1) X-ray diffraction (XRD); (2) X-ray fluorescence (XRF); (3) Optical microscopy using reflected light; (4) Scanning electron microscope (SEM); and (5) Electron microprobe. Frozen solid samples were thawed in an oven at 40 °C and then dried and stored in a vacuum bottle before analysis. Dried samples, consisting mostly of well-crystalline sulfide solids (see the section "Laboratory Analysis of Biogenic Solid"), appear to remain stable in the vacuum bottle. Dried powders were then analyzed by a Bruker D2 Phaser X-ray Diffractometer. The mineral composition of the samples were determined by a peak search and match procedure using DIFFRAC.EVA software. Bulk samples of the powders were also analyzed by a portable Bruker Elemental Tracer IV-ED XRF for semi-quantitative measurements. After XRF analyses, sample powders were imbedded in epoxy, ground, and polished with diamond paste and investigated in reflected light using a Nikon Labophot research polarizing microscope. Powder samples were then mounted and sputter-coated for investigation in three-dimensions using a Zeiss EVO 50VP SEM at Auburn University. Arsenic contents in polished pyrite solids were quantified more precisely using a JEOL 8600 electron microprobe at Auburn University. Quantitative analyses were performed with wavelength dispersive spectrometers (WDS) automated with the Probe for EPMA software (Advanced Microbeam), and standards for Fe, S, and As. Finally, the sulfur isotope signatures of dissolved sulfate were measured to fingerprint the progress of bacterial sulfate reduction in treated groundwater. Dissolved SO_4 was precipitated out of water samples as $BaSO_4$ by addition of excess $BaCl_2$. SRB have a well-known kinetic isotope effect on dissolved sulfate (Thode, Kleerekoper, and McElcheran 1951). The aqueous $\delta^{34}S$ values were measured at the Colorado Plateau Stable Isotope Laboratory at Northern Arizona University using standard combustion techniques and analyzed by a Thermo Electron gas isotope-ratio mass spectrometer.

Microbiology analysis

The total DNA of each aqueous slurry sample collected from the wells was extracted by using Powersoil® DNA isolation kit (MO BIO, Carlsbad, CA, USA) following the manufacturer's instruction. The concentrations of the total sulfate-reducing bacteria (SRB) were determined through real-time PCR targeting the *apsA* gene (Ben-Dov, Brenner, and Kushmaro 2007). DNA samples extracted from known concentrations of an ATCC reference strain, *Desulfovibrio vulgaris subsp. vulgaris* (ATCC 29579), were used to establish the standard curve for calculation. Real-time PCR was carried out using PerfeCTa SYBR® Green SuperMix (Quanta, Gaithersburg, MD, USA) and on ABI 7500 (Applied Biosystems, Foster city, CA, USA).

Arsenic speciation analysis

For arsenic speciation analysis, water sample was first filtered with a 0.45-μm filter then filtered through a disposable arsenic speciation cartridge

(Meng and Wang 1998). For separation of the arsenic species, the cartridge was attached to a 50-mL syringe (with luer slip tip) filled with the water sample. When water is filtered through the arsenic speciation cartridge, the first 5 mL of the filtrate was discarded before collecting the samples. As speciation cartridges contain an highly selective aluminosilicate adsorbent that adsorbs the negatively charged arsenic species (or As(V), such as $H_2AsO_4^-$) and allows the uncharged arsenic species (As(III), H_3AsO_3) to pass through. As(III) is then measured in the effluent filtered through the cartridges and As(V) is calculated as the difference between total As and As(III). Thioarsenite aqueous complexes are not analyzed due to the lack of certified standards.

Geochemical modeling: Speciation and saturation index calculations, reaction path models

Geochemist's Workbench (Bethke 2008) was used to calculate 1) the speciation of arsenic under various Eh–pH conditions, 2) time change of saturation index of arsenian pyrite at field site, and 3) mineralogic reactions, arsenic concentrations, and groundwater chemistry changes in response to field biostimulation of $FeSO_4$ amendments. Thermodynamic data for thioarsenite species, amorphous As and Fe sulfide phases, and arsenian pyrite (Saunders et al., 2008) were compiled into a revised GWB database for the speciation calculations.

Patented technology

Authors were granted two US patents (Saunders 1996; Lee, Saunders and Nichols 2008) designed to remove and sequester arsenic and trace metals in contaminated groundwaters. The in situ method utilizes a treatment solution comprising a biodegradable source of organic carbon, ferrous iron, and sulfate. Additionally, the treatment solution may comprise SRB as well as nutrients to enhance bacterial metabolism. The treatment is designed to stimulate the growth of naturally occurring SRB such that arsenic and trace metals are adsorbed and co-precipitated in iron sulfide solids and the hydrocarbons are reduced to innocuous byproducts. SRB activities generate a subsurface bio-mineralization zone surrounding the well to sequester mobile contaminants when water is subsequently drawn through the well.

Geologic background of study area

Shallow groundwater and sediments at the industrial site contains elevated levels of arsenic derived from herbicide applied at the surface. From 1989 to 1993, contamination assessments verified that contamination level in groundwater was well above EPA limit of 0.05 mg/L and had spread off-site (Starnes, 2015). Initial remediation began in 1992 with the excavation of approximately 590 cubic meters of contaminated soil. This directly led to a 40% decrease in the arsenic concentration. This excavation was followed by the installation of a pump-and-treat system to further the remediation effort. Though the pump-and-treat system was successful in remediating the off-site plume, it reached a point of diminishing returns on-site prior to achieving site remediation standards, so was discontinued in 1999.

The industrial site is located within the Gulf Coastal Plain of the Florida panhandle, where thick sequences of marine sediments are deposited underneath the area within the Apalachicola Embayment. The Florida panhandle falls within the East Gulf Coastal Plain section of the Coastal Plain physiographic province. The oldest rocks found in outcrops exposed in the area are Early Miocene limestone units. The youngest rocks found in the county are Pleistocene to Holocene undifferentiated quartz sands, clayey sands, and gravels. These sands overlie the limestone units which can extend to depths of 900 m, and below the limestone units, sandstones and shales extend to granitic basement rock (Schmidt and Clark 1980).

There are four major hydrogeologic units that are generally recognized in the state of Florida: the surficial aquifer system, the intermediate confining unit, the Floridan aquifer system, and the sub-Floridan confining unit. The surficial aquifer system is made up of undifferentiated terrace-marine and fluvial deposits in the northern Florida panhandle and normally consists of clayey sands and gravels near the coast. Specifically in the study area, the surficial aquifer is mainly composed of quartz sand and gravel with occasional clayey sand

and sandy clay lenses and extends from the surface to a depth of approximately 6–7.6 m. In the surficial aquifer, the water table typically occurs at approximately 1.5 m below the surface. Due to the shallow groundwater table and flat topography, modeling results show that groundwater flow direction can change with precipitation events (Starnes 2015). Historically at the site, groundwater flow direction has been to the northwest and west from the site and it migrates at an average rate of about 20 m per year. Organic material that manifests as dark brown zones is present in the surficial aquifer (Schmidt and Clarke 1980). There is a 0.9–1.5 m thick, laterally continuous layer of organic material in the quartz sand at a depth of about 1.5–3 m. This layer has been observed to thicken to the north (Schmidt and Clarke 1980). Groundwater from the surficial aquifer discharges into local streams or springs, or it may migrate into the deeper Floridan aquifer system where the two aquifer systems are hydraulically interconnected.

Underlying the surficial aquifer is the Jackson Bluff Formation, which is an important intermediate confining unit that separates the surficial aquifer from the intermediate aquifer. This unit acts as a barrier, restricting flow from the Surficial Aquifer downward to the other hydrostratigraphic units (Schmidt and Clark 1980). Consequently, this restricts the advective transport of arsenic downward to the other hydrologic facies and helps confine the contamination to the Surficial Aquifer (Schmidt and Clark, 1980). The Jackson Bluff Formation is characterized as sandy clay to clayey sand possessing large portions of mollusk shells and occurs from approximate depths of 6–9.15 m, and ranges from thicknesses of 1.5–2 m (Schmidt and Clark 1980). Because of its irregular deposition and erosion, the Jackson Bluff Formation occurs intermittently in the study area, but is present on site.

Results and discussion

Field parameters

Field parameters and water chemistry changes significantly in injection wells and near-by monitoring wells at the site (Tables S1–S11 in Supplementary Material). ORP values before the injection showed mildly reducing conditions (44.4 ± 63.6 mV). One week after the injection, the ORP values (Table S1 in Supplementary Material) dropped significantly (below -120 mV) in injection wells and affected monitoring wells M-1 and M-2. These low ORP values indicate that sulfate-reducing conditions were quickly established in the aquifer 1 week after injection, which is confirmed by quantitative microbiology analysis that show significantly higher amount of SRB after injection (see the section "Microbial Changes"). Also from a microbiology stand point, perhaps SRB began to out compete Fe-reducing bacteria by dropping the ORP/Eh (Chapelle and Lovley 1992). The ORP values remained negative in all affected wells months after the injection, implying that the reducing conditions were maintained with a parallel decrease in arsenic concentrations, which is discussed below.

The dissolved ferrous iron concentration increased significantly to the highest values of 54 and 138 mg/L in I-2 and I-2 2 weeks after the injection of ferrous sulfate (Table S2 in Supplementary Material). A minor contributor to the increase in ferrous iron may have been caused by bacterial iron reduction, which often occurs prior to sulfate-reducing conditions under moderately reducing condition (Saunders et al. 2008; Chapelle and Lovley 1992). Dissolved H_2S concentrations in groundwater (Table S3 in Supplementary Material) increased significantly to several mg/L in injection wells and affected monitoring wells as compared to their pre-injection levels (<0.1 mg/L). However, as sulfate-reducing conditions quickly established, and subsequent precipitation of iron sulfide from the groundwater (see below), both ferrous iron and H_2S concentrations decreased significantly to near the pre-injection levels, several months after the injection.

Phase diagrams for arsenic speciation in the presence of S and Fe were calculated using the ACT2 sub-program of Geochemist's Workbench (Bethke 2008) with added thermodynamic data for thoiarsenite species and arsenian pyrite (Saunders et al. 2008). In the arsenic-sulfur-iron system (Figure 3), arsenian pyrite replaces arsenic sulfide solids and thoiarsenite species as the most stable phase under reducing conditions. Significant drops in groundwater Eh values were

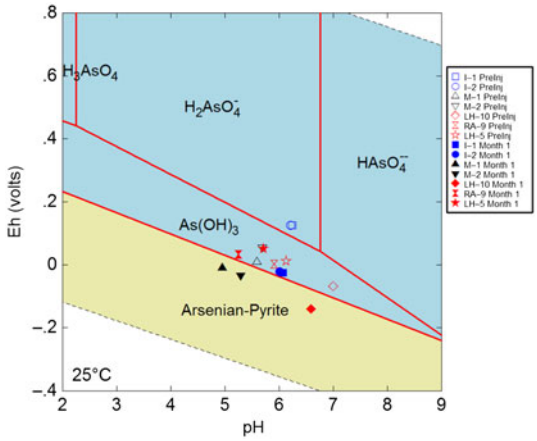

Figure 3. Eh–pH diagram calculated for As–Fe–S system at 25 °C and fixed As, Fe^{2+}, and SO_4^{2-} activities of 10^{-6}, 10^{-4}, and 10^{-5}, respectively. The results show the stability field of different arsenic species under different geochemical condition. Also plotted are the Eh and pH values of groundwater measured for pre-injection and 1 month after the injection. Plot was constructed using Geochemist's Workbench.

observed in affected wells (M-1, M-2, and LH-10) after the injection, which would favor the precipitation of arsenian pyrite solids under reducing conditions (Figure 3). The pH values of affected wells were found to be between 5 and 7 for a majority of the study period, previous laboratory sorption experiments (Farquhar et al. 2002) suggested that this pH range was favorable for arsenic sorption onto pyrite. The formation of arsenian pyrite, which removes dissolved arsenic from groundwater, is confirmed by our laboratory analysis (see below).

Laboratory geochemical data of water samples

The DOC levels in injection wells (I-1 and I-2) and two nearest downgradient wells (M-1, M-2) increased up to hundreds of mg/L 1 week after injection (Table S4 in Supplementary Material). The elevated DOC concentrations in these wells dropped to pre-injection levels when the bulk of organic carbon was consumed by SRB. However, a delayed increase in DOC (>100 mg/L) was observed in the monitoring well LH-10 as the injected plume migrated further downgradient. These results indicate that DOC levels in groundwater can be used to trace the changes in total organic loading in groundwater (compounds <0.45 μm in diameter) and subsequent biodegradation after injection. Phosphate and nitrate concentrations (Tables S5–S6 in Supplementary Material) also increased significantly in injection wells and monitoring wells M-1 and M-2 1 week after the injection compared to pre-injection levels (0.12 ± 0.04 mg/L for P and 0.049 ± 0.005 mg/L for total nitrate). Total nitrate and phosphate levels, similar to DOC, started to decrease the second week after the injection as apparently they were consumed by bacterial metabolism.

Arsenic concentrations increased to several mg/L in affected downgradient wells (M-1, M-2) 2 weeks after the injection, but began to decrease from the third week (Figure 4 and Table S7 in Supplementary Material). After a few weeks, arsenic levels in three affected wells decreased significantly from 0.25-0.34 mg/L to below 0.05 mg/L (Figure 5). After about 1 month, the site regulatory clean-up goal for arsenic of 0.05 mg/L had been reached in all three affected wells, and remained below that for at least 6 months in M-1 and M-2. Arsenic concentration in the deeper LH-10 well dropped below 0.05 mg/L over the entire year of monitoring after injection. Tables S7 and S8 in Supplementary Material show that As(III) is the dominant dissolved arsenic species in the groundwater, as expected under reducing conditions.The total Fe concentrations in M-1 and M-2 increased to more than 100 mg/L 1 week after injection (Figure 5 and Table S9 in Supplementary Material) compared to the pre-injection levels (< 1 mg). Dissolved sulfate concentrations in these wells also increase to hundreds of mg/L after injection (Figure 5 and Table S10 in Supplementary Material). The concurrent increase in arsenic and ferrous iron concentrations right after injection might be resulting from bacterial iron reduction. Iron-reducing bacteria compete with SRB for organic carbon and they can cause arsenic release (Chapelle and Lovley 1992). Amendments of nutrients in wells might also cause initial arsenic release because phosphate and nitrate can compete with arsenic for sorbing sites on aquifer minerals (Neumann et al. 2010; Aziz et al. 2017). Fe, SO_4, and As levels in affected wells show concurrent decreases in the third week, followed by decrease in H_2S in the fourth week, indicating that SRB were causing the precipitation of pyrite and removal of arsenic from groundwater (Figure 5). Thus H_2S produced

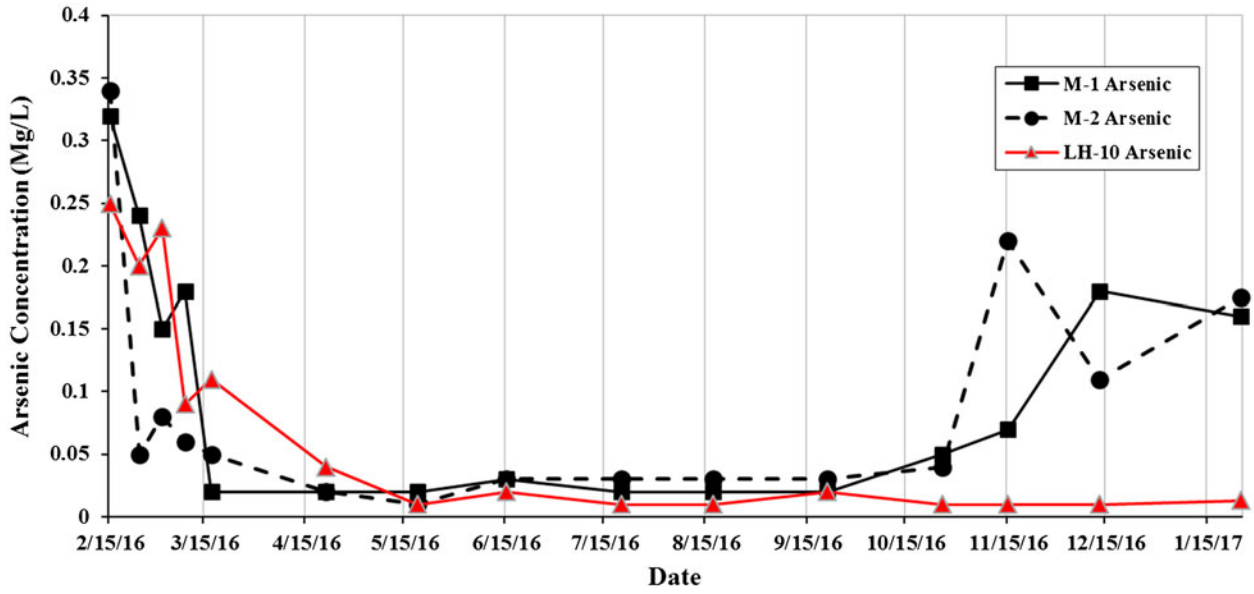

Figure 4. Plot showing changes of arsenic concentrations in three downgradient wells (M-1, M-2, and LH-10) after injection (solid lines), arsenic level these wells dropped below the regulatory cleanup goal for arsenic concentration at the field site (0.05 mg/L) after about 2 months when sulfate reduction conditions are established.

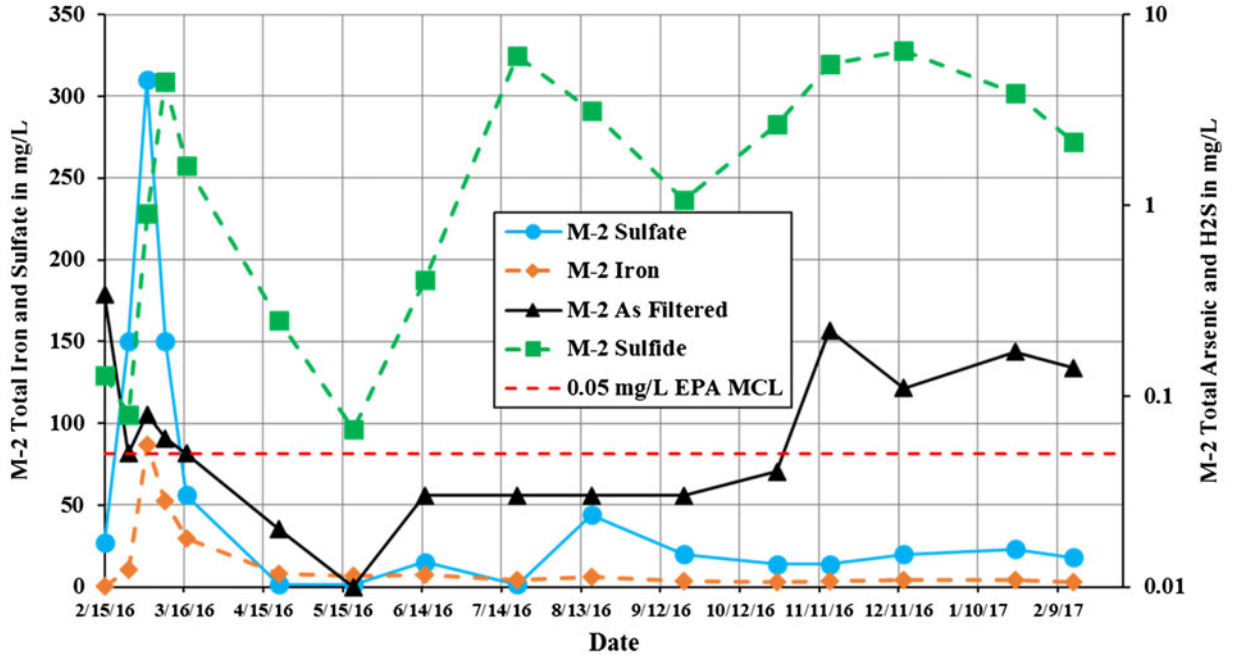

Figure 5. Plot showing time series groundwater geochemical data (dissolved) from monitoring well M-2 at the field site, which is located ~1.5 m from a bioremediation injection well. The initial spikes in Fe, SO_4 are due to their concentrations in the injected solution, and dissolved H_2S spike occurs shortly after as biogenic sulfate-reduction begins. Time-related decreases in Fe, H_2S, and As are interpreted here to be the result of precipitation of arsenian pyrite. Dashed red line is the regulatory cleanup goal (0.05 mg/L) for arsenic concentration at the field site.

by SRB apparently reacted with dissolved Fe (or perhaps Fe in solid phases) to make pyrite capable of removing arsenic by sorption and co-precipitation. The nitrate and phosphate concentrations also decrease during this period (not shown), suggesting that SRB utilize them in their metabolism process. These results indicate that although the important ingredients for SRB growth (i.e., DOC, Fe, SO_4, and nutrients) returned back to the pre-injection levels after a few months, the newly formed iron sulfide minerals remain stable for arsenic sequestration.

Spatial and temporal geochemical changes

During the injection experiment, chloride in the injected fertilizer served as a conservative tracer (Table S11 in Supplementary Material) to determine average groundwater velocity and assess how much arsenic removal is achieved via biomineralization, or by injection mixing. The analysis was performed through the use of chloride breakthrough curves along a flow transect of wells I-1, M-1, LH-10, and RA-9 (Figure 6). Chloride concentration in the initial injectate was 200 mg/L. Advection and diffusion are considered as the main process responsible for the movement of conservative tracers. Given the average hydraulic conductivity of about 400–500 m/year, hydraulic gradient of 0.010-0.015, and porosity of 30% at the site, the estimated flow velocity is about 20 m/year. Assuming advective transport, the peaks of chloride tracer arrived M-1, LH-10, and RA-9 around 30, 75 and 175 days after tracer injection. Thus the results of conservative tracer test (Figure 6) is consistent with the average velocity estimated by Darcy's Law, although the chloride tracer likely moved faster near the injection points by greater hydraulic gradients. Decreases in chloride concentration as the tracer moved downgradient (Figure 6) were likely caused by dilution and diffusion. Figure 7 shows the calculated fraction of arsenic removal (with respect to pre-injection levels) and fluid mixing ratio (the volume of injectate that is in per volume of groundwater) in monitoring wells M-1 and M-2 over time. The mixing ratio w is calculated as follows:

$$w = \frac{C_{mixed} - C_{pre-injection}}{C_{injectate} - C_{mixed}}$$

where C_{mixed}, $C_{\text{pre-injection}}$, and $C_{\text{injectate}}$ are chloride concentrations in the mixed fluid, pre-injection groundwater, and injectate. The results show that more than 90% of dissolved arsenic were removed from groundwater in both wells during the main sequestration stage between April and September, while during the same period the mixing ratios remained below 0.2 in M-1 (with large volume of injection) and below 0.1 in

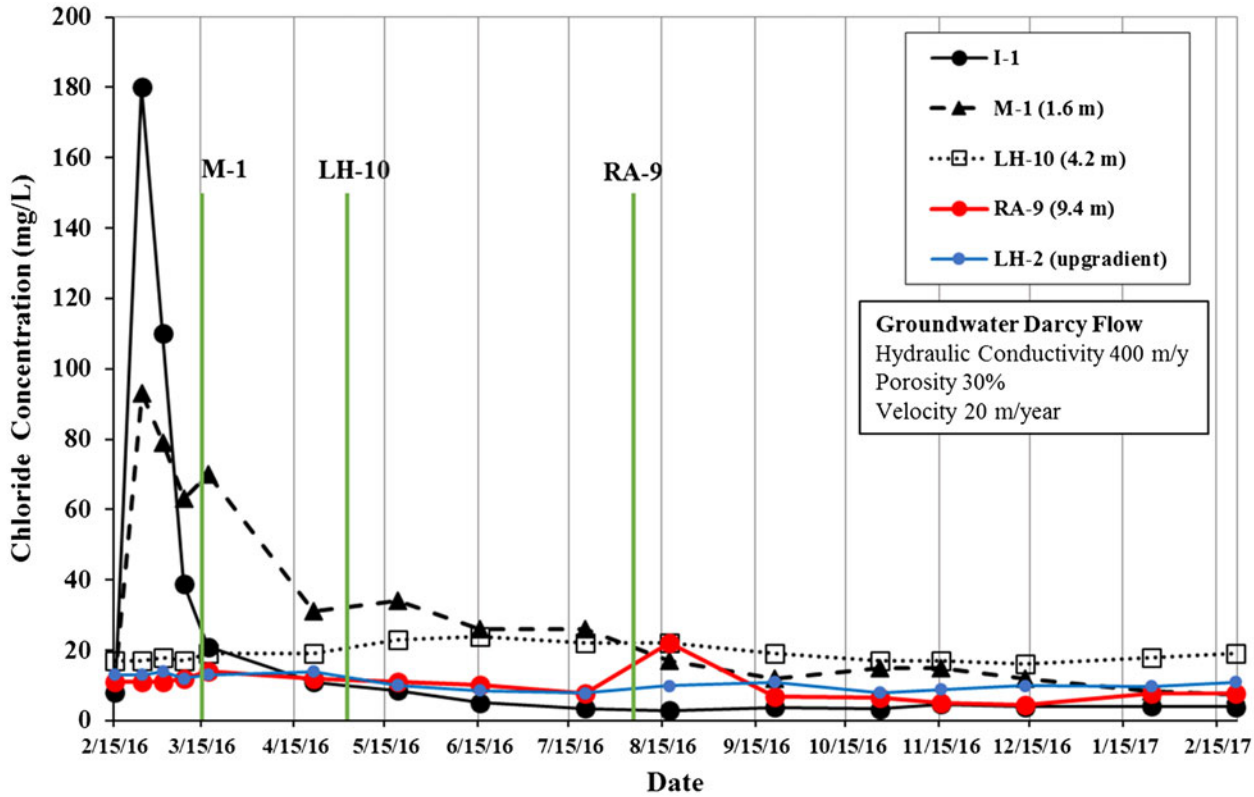

Figure 6. Plot showing breakthrough curves showing time-series changes in chloride tracer concentrations along the I-1, M-1, LH-10, and RA-9 flow transect. Green lines show the estimated peak arrivals at various wells based on calculated Darcy flow velocity. LH-2 is an unaffected up-gradient well.

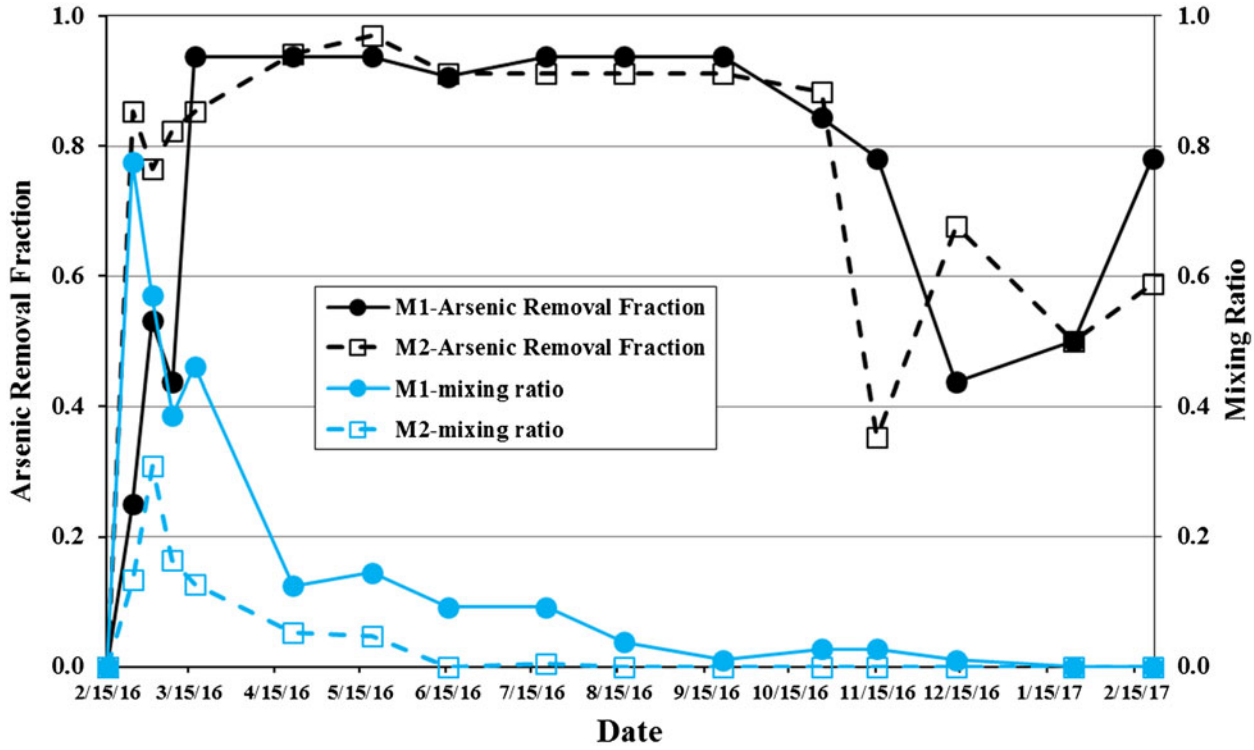

Figure 7. Plot showing time-series changes in arsenic removal fraction and fluid mixing ratio (injectate volume: groundwater volume) in M-1 and M-2 wells. These values were used as the primary metric for assessing relative effects of bio-mineralization and mixing on arsenic removal.

M-2. Thus dilution accounted for less than 20% of total arsenic removal. Clearly the stimulated bio-mineralization and accompanying co-precipitation and sorption processes accounted for more than 80% of overall arsenic removal.

The saturation index (SI = log IAP/log K) of arsenian pyrite in groundwater was calculated to assess the geochemical conditions for its potential precipitation along a flow transect of wells I-1, M-1, LH-10, and RA-9 (Figure 8). The results show that groundwater in these wells was undersaturated (with negative SI values) with respect to the mineral phase arsenian pyrite prior to injection. Arsenian pyrite quickly became oversaturated in I-1 and M-1 in 1 week due to the addition of injected iron and sulfate. The injection also caused a short-lived (in Week 1) pyrite saturation in the adjacent up-gradient well LH-2. After 2 months, the injectate reached well LH-10 further downgradient and significantly increased pyrite SI there. The pyrite SI remains mostly positive in M-1, M-2, and LH-10 wells during the 1-year monitoring period; such trends support that the arsenic sequestration was effectively maintained by the formation and stability of arsenian pyrite. This result is confirmed by XRD analysis of solids recovered from wells (see the section "Laboratory Analysis of Biogenic Solids").

Figures 9 and 10 show the changes in arsenic concentrations and water table elevations, precipitation, and ORP values in affected wells M-1, M-2, and LH-10 during the 1-year monitoring period. In general, rainfall causes the water table and ORP to rise (Figure 9). Despite the fluctuations in water table and ORP, arsenic concentrations remained below the regulation level of 0.05 mg/L in these affected wells for at least 6 months (from March to September) (Figure 10). After the 6 month principal sequestration stage, rainfall-induced short-lived changes in arsenic level became noticeable. The dry period between early October and December allowed the water table to drop, which perhaps caused a short-lived oxidation of sulfide solids and remobilization of arsenic (Figure 10). However, the observed arsenic increases in M-1 and M-2 were not accompanied by concurrent increases in Fe or SO_4, suggesting limited oxidation of biogenic pyrite. Previous lab experiments (Couture et al. 2013) showed that only around 2% of previously

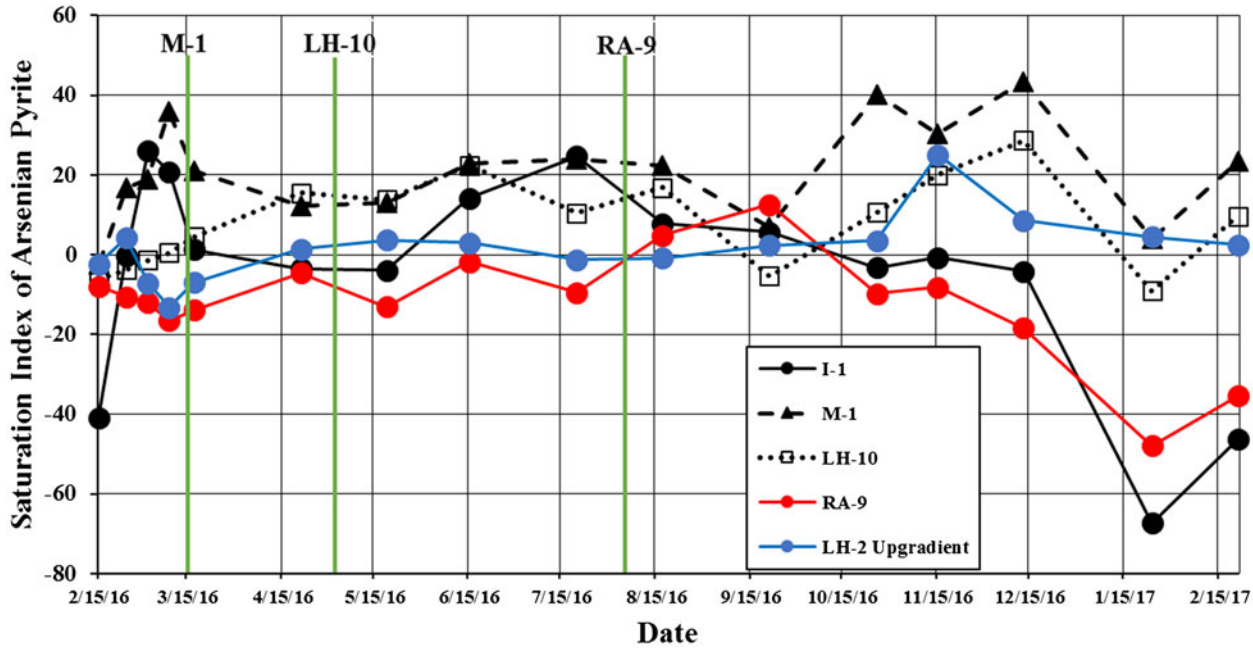

Figure 8. Calculated saturation index (SI) of arsenian pyrite in groundwater along the I-1, M-1, LH-10, and RA-9 flow transect. Green lines show the estimated peak arrivals at various wells based on calculated Darcy flow velocity.

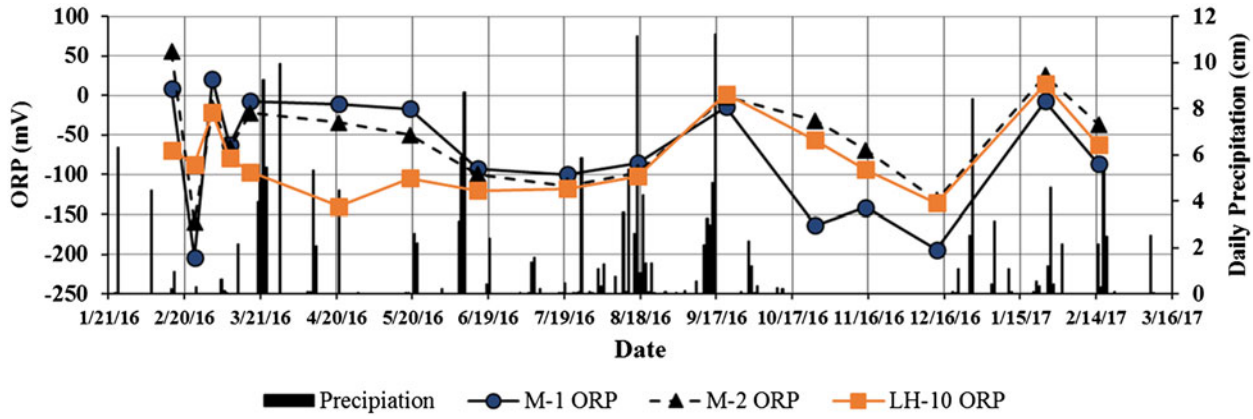

Figure 9. Plot of time-series data of ORP and precipitation in M-1, M-2, and LH-10 wells. Precipitation data were gathered from a weather station located about 8.75 miles (14.11 km) from the field site (Data source: NOAA's National Center for Environmental Information, www.ncdc.noaa.gov).

sequestered arsenic in pyrite re-dissolve into solution under aerobic conditions. As discussed above, groundwater migrates at the rate of about 20 m per year in a general direction from southeast to west-northwest. Thus the arrival of untreated groundwater from up-gradient (i.e., from southeast) would also cause an increase in arsenic concentrations during the latter part of the experiment. Overall, the arsenic concentrations after September were still below the pre-injection level in affected wells. The arsenic levels in the LH-10 well did not show a significant shift in response to hydrologic or meteorological changes. This could be due to its relatively deeper water table that is less sensitive to precipitation (Figure 10).

Laboratory analysis of biogenic solids

The solid slurry samples were collected from each well for the duration of the yearlong study. The sediments accumulated through gravity settling in the bottom of the wells, using a peristatic pump and silicone tubing these sediments were collected placed in 1-L plastic bottles. These bottles were immediately placed in coolers containing dry ice

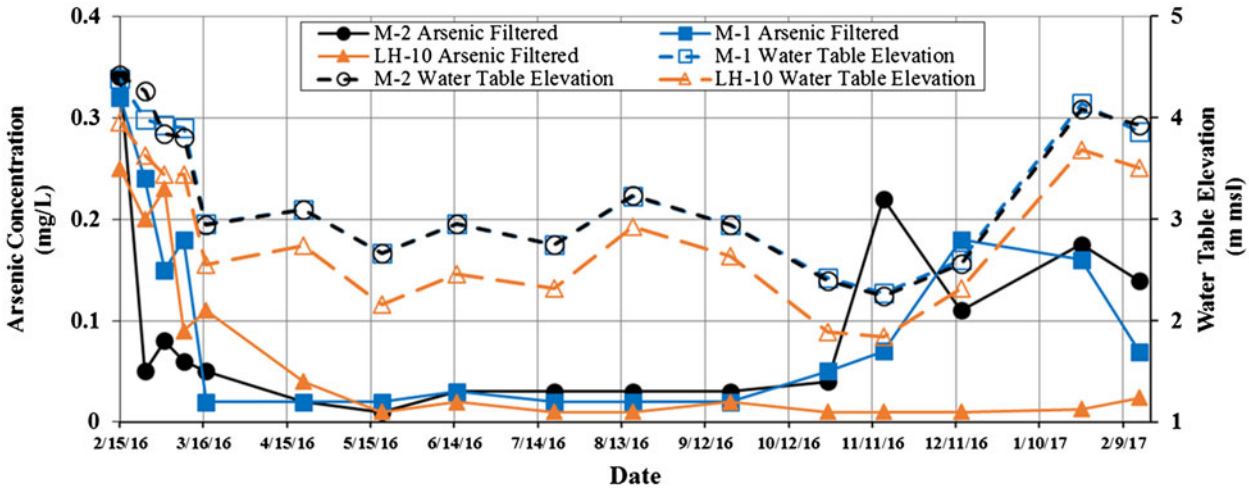

Figure 10. Plot showing changes of arsenic concentrations in three downgradient wells (M-1, M-2, and LH10) after injection (solid lines), arsenic level these wells dropped below the regulatory cleanup goal for arsenic concentration at the field site (0.05 mg/L) after about 2 months when sulfate reduction conditions are established. Also shown are changes in water table elevation in wells (dashed lines).

with limited headspace (to preserved redox conditions). These bottles were stored in a freezer until the sediments were processed. The processing of these sediments begins by first thawing and dewatering the bottles taken from the field. The dewatering process was conducted in two different ways. The first method of dewatering was conducted by transferring as much solid particulates from the 1-L bottles to much smaller 50 mL centrifuge vials. The vials, labeled with the specific well the sediments were collected from, were then centrifuged for approximately 10 min at 3000 rotations per minute (rpm). Once centrifuged the excess liquid was drained, the wet sediments were transferred to ceramic crucibles to be subsequently dried on a hotplate, and transferred to small, labeled plastic bags. This would often take several days for the sediments to completely dry using this method. The other method of dewatering consisted of pouring the thawed sediment slurry through Whatman Grade 2, 8-µm pore sized filter paper. The filter paper was then dried on a hotplate and the sediment transferred to small, labeled plastic bags. This filter dry method took around a day for the sediments to completely dry. After drying the sediments are ready for imaging and geochemical analysis. Though sediments were collected from all 10 wells, the sediments collected from the injection wells (I-1, I-2) and wells closest in proximity to the injection wells (M-1, M-2), were the focus of this analysis.

The sediments were first analyzed by X-ray diffraction (XRD). The results from wells M-1 (Figure 11) show well-defined peaks that closely match arsenian-pyrite (at $2\theta = 28.5°$, 33.0°, 37.0°, 40.7°, 47.3°, 56.2°), as reported from lignite from Czech Republic (Rieder et al. 2007). The intensities and sharpness of peaks for arsenian pyrite that formed during the very early stage of the experiment (i.e., March 2nd or about 2 weeks after injection) were not as pronounced as those formed later (after April, Figure 11). Pyrite precursors such as amorphous iron sulfide or mackinawite were not found in our XRD analysis at any stages (see discussion below). Interestingly the major peaks of pyrite collected 1 year after the injection (February 15, 2017) still remain their strong intensity and sharpness (Figure 11), implying that pyrite remains stable in the treated aquifers during the entire experiment. Pyrite grains are isotropic and they occurred as crystals and framboids (spherical aggregates of pyrite nanoparticles) ~ 1-10 µm in size. No other crystalline Fe–S or As–S phases was detected optically or by XRD. SEM images (Figure 12) further confirmed that pyrite occurred either as well-formed octahedral crystals or framboids, and they were commonly attached to the silicate phases from the aquifer. Octahedral morphology and framboidal particles dominated in samples collected over time, including during the later stage of the experiment. Morphologically similar pyrite has

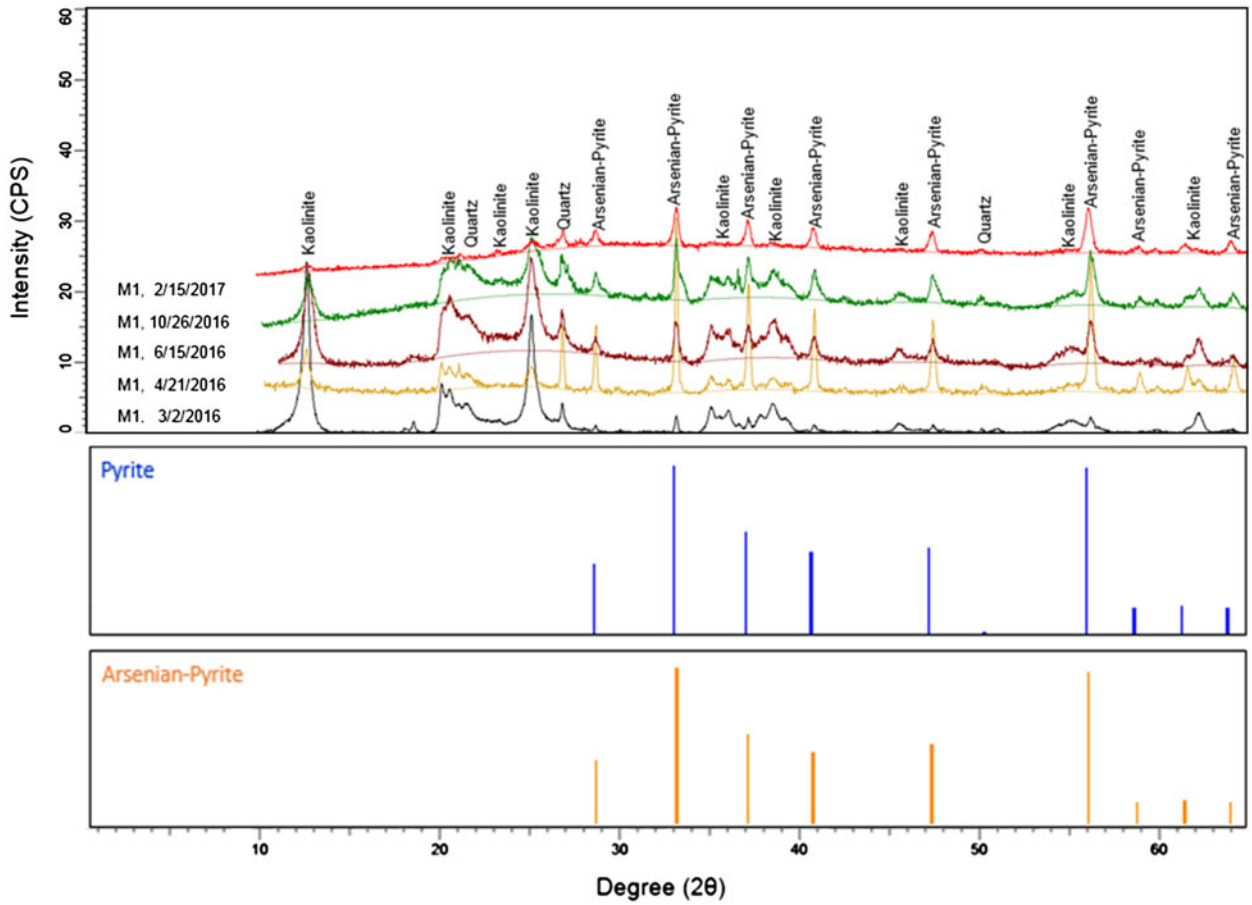

Figure 11. XRD spectrum of solid samples recovered from monitoring well M-1 well over 1 year of experiment. Major peaks of iron minerals closely match arsenian-pyrite peaks from Rieder et al (2007). The background level of counts per second (CPS) of different spectrum was shifted for visual comparison.

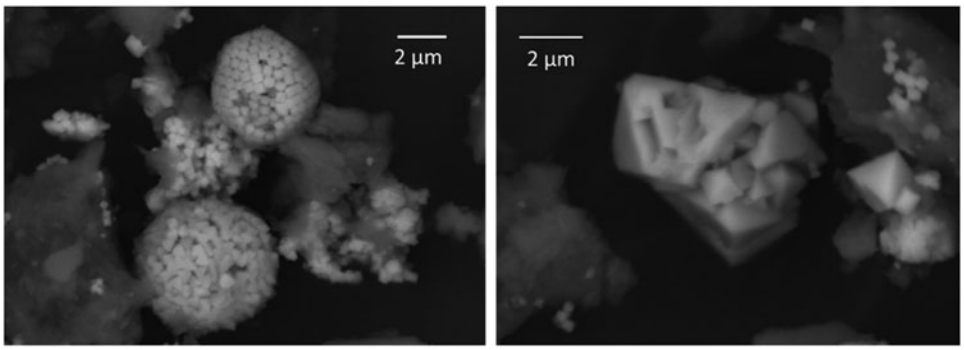

Figure 12. SEM backscatter images of biogenic arsenian pyrite crystal (right) and framboids (left) and associated aquifer silicate minerals (grey). These mineral aggregates were recovered from slurries at the bottom of injection well I-2 at the site 1 month after the injection. These nanoparticles formed during field stimulation of natural sulfate-reducing bacteria in the aquifer.

been successfully synthesized in the laboratory using Fe(II) and H_2S as initial reactants (Gartman and Luther 2013), implying a rapid pyrite formation over a very short synthesis time period (<12 h).

XRF analysis of solids consistently results in peaks for Fe, S, and As (Figure 13), which is consistent with XRD spectrum and petrographic analysis that a single Fe-S-As solid phase was formed by bacterial sulfate reduction. The results also imply that pure As–S phases such as realgar and orpiment are not likely to form in Fe-rich, low-temperature environments at circum-neutral pH. Arsenic contents in polished pyrite grains

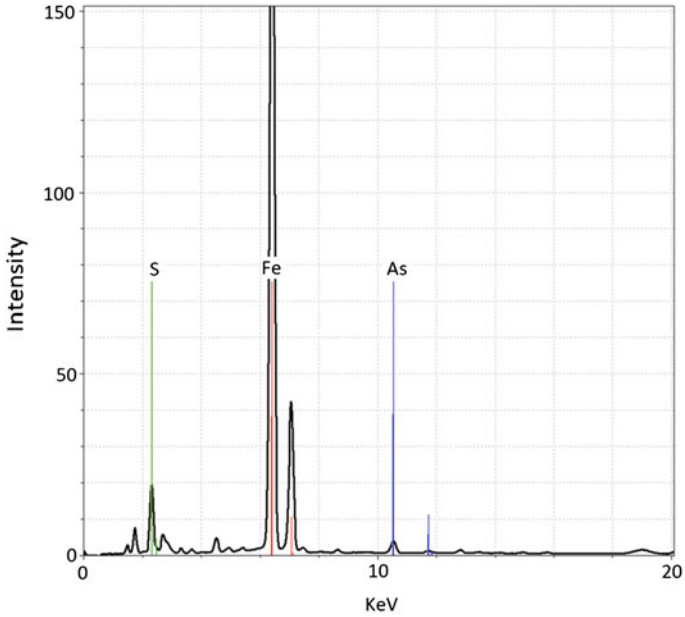

Figure 13. XRF spectrum of solid samples recovered from monitoring well M-2 1 month after the injection. Similar spectrum was observed in other affected wells (not shown). The peaks for As, S, and Fe show the presence of these elements in the solid phase.

were quantified using a JEOL 8600 electron microprobe. Microprobe results confirmed that the pyrite solids formed were arsenian pyrite containing 0.05 to 0.4 wt. % of arsenic (Figure S1 in Supplementary Material). The percentage range is significantly higher than the level of arsenic (typically in the range of a few mg/L) in fluvial sediments (Shamsudduha et al. 2008; Lee et al. 2007; Horneman et al. 2004), implying excellent sequestration capacity of biogenic pyrite formed. Finally, groundwater experienced the most active bacterial sulfate reduction (as evidenced by high SO_4 and H_2S in groundwater) tend to be enriched in heavy ^{34}S (range from 2.02 to 4.00 ‰) compared to unaffected well water (0.40–0.61 ‰) or sulfur in injected $FeSO_4$ (0.44–0.66 ‰) (Figure 14). Because SRB preferentially use the lighter ^{32}S in producing H_2S gas, such fractionation leads to enrichment of ^{34}S in the remaining dissolved sulfate relative to H_2S produced. This observed trend is consistent with S isotope fractionation attending bacteria sulfate reduction (Thode, Kleerekoper, and McElcheran, 1951).

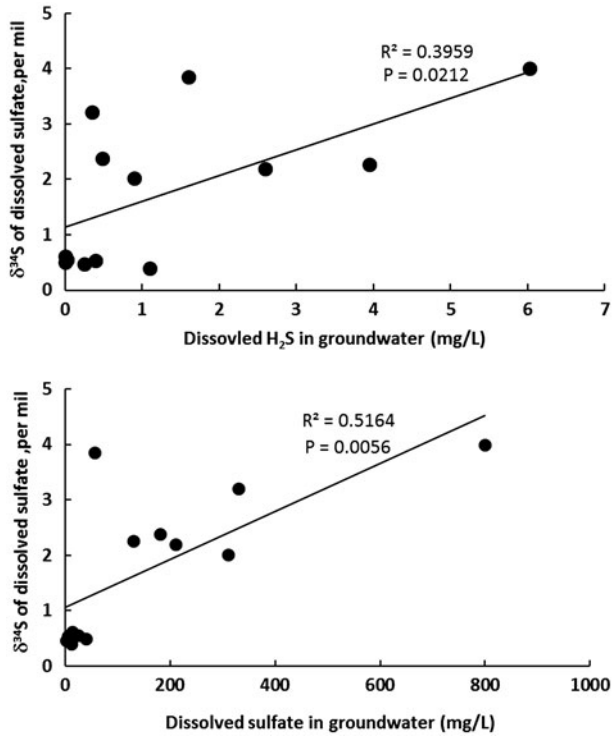

Figure 14. Plots showing sulfur isotopic composition of dissolved sulfate (in ‰, relative to Canyon Diablo meteorite, CDT) vs. (a) H_2S and (b) dissolved sulfate concentration during bioremediation experiment.

Microbial changes

The changes in concentrations of the total SRB (SRB) aqueous slurry samples were determined through real-time PCR by targeting the *apsA* gene. Results showed that while the concentrations of SRB present in the pre-injection samples were below the limit of detection (1.01 Log_{10} copies/µl), samples of both injection wells and monitoring wells (M1, M2, I1 and I2) contained

significantly higher amount of SRB for at least 2 months after injection (Figure S2 in Supplementary Material). The concentrations of SRB DNA in those samples reach approximately 3 Log_{10} copies/µl. Quantitative PCR analysis confirmed that SRB activities were enhanced by amendment of organic carbon. Our method detects the adenosine-5'-phosphosulfate and the results show *Desulfovibrio spp.*, *Desulfotomaculum spp.* and other soil-rich SRB could be the functional SRB in the samples.

Geochemical reaction modeling

Geochemical modeling was conducted using GWB (Bethke 2008) to assess speciation of arsenic, predict mineralogical reactions along reaction paths, and estimate the arsenic sequestration potential of arsenian-pyrite under site specific conditions. Figure 1 shows that under oxidizing conditions $H_2AsO_4^-$ and H_3AsO_4 are dominant at low pH (<7) while $HAsO_4^{2-}$ and AsO_4^{3-} become dominant at higher pH. Under moderately reducing conditions H_3AsO_3 predominate over a wide range of pH values. In sulfur-rich systems, solid arsenic sulfides (orpiment) or thioarsenite aqueous complexes ($As(SH)_4^-$ and AsS_3^{3-}) become the dominant phases under reducing conditions, When the system contains sufficient iron, arsenian pyrite replaces thioarsenite aqueous complexes and become the most thermodynamically stable arsenic phase under highly reducing conditions.

The next sets of reactions were modeled using GWB's React program. The purpose of these reaction path models was to predict changes in dominant mineralogy and arsenic concentrations under sliding Eh conditions, before and after the addition of $FeSO_4$ to the aquifer at the site-specific conditions. The pre-injection groundwater geochemistry of well I-1 was used to set the initial condition for the simulations. Table S12 in Supplementary Material shows the observed changes in arsenic content and water chemistry over the 1-year monitoring period. The initial groundwater contains about 190 µg/L of dissolved arsenic. The GWB traces the mineralogical reactions and water chemistry changes as the Eh values slide from 0.15 V to -0.15 V. The predicted mineralogical changes are shown in Figure S3 in Supplementary Material. As the system transitions from oxidizing to reducing conditions there is a shift in dominant mineralogy from hematite to arsenian-pyrite at an Eh of -.05 V. The arsenian-pyrite is given as follows:

$$SO_4^{2-} + 2CH_2O + 2H^+ \rightarrow H_2S + H_2CO_3$$

$$Fe^{2+} + 1.995\ H_2S + 0.01\ As(OH)_4^- + 2H^+ \rightarrow FeS_{1.99}As_{0.01} + 1.02\ H_2O + 3.5\ O_2(aq)$$

This precipitation of arsenian-pyrite of about 10^{-5} mol in 1 kg solution results in only about 20 µg/L decrease in the dissolved arsenic concentration (from 190 to 170 µg/L) in groundwater at the end of reaction path. These results demonstrates that precipitation of arsenian-pyrite in response to Eh drops at the site would not lower arsenic concentrations below the EPA's MCL of 10 µg/L, amendments of $FeSO_4$ is required to increase the amount of pyrite precipitation and arsenic sequestration.

The second reaction path model (Figure S4 in Supplementary Material) was created to predict how much $FeSO_4$ would need to be added to this system to form enough arsenian-pyrite to drive the arsenic concentration below the EPA limit of 10 µg/L. In this model, the GWB traces the mineralogical reactions and water chemistry changes as 2.47 mmol of $FeSO_4$ was added into 1 kg of initial I-1 groundwater and Eh values slide from +0.5 V to –0.2 V. In this simulation, more thermodynamic stable hematite phase is replaced by amorphous $Fe(OH)_3$ in the initial system. The amendments of $FeSO_4$ would increase the concentrations of Fe^{2+} and SO_4^{2-} in the ground water from 0.47 mg/L and 16 mg/L (pre-injection groundwater concentrations) to 40 mg/L and 60 mg/L, respectively. The modeling results show that significantly more (10^{-4} mol) of arsenian-pyrite forms from per kg of solution to sequester arsenic compared to the case without amendments (Figure S4 in Supplementary Material). The groundwater arsenic concentration drops significantly from 190 µg/L to below the EPA's MCL of 10 µg/L (Figure S5 in Supplementary Material). This modeling results indicate that $FeSO_4$ amendments is necessary to sequester arsenic below EPA's MCL at the site investigated, which is

consistent with the field results. The geochemical modeling techniques can help quantify the $FeSO_4$ amendments required to sequester arsenic below EPA's MCL. The dominant mineralogy shifts from an iron oxy-hydroxide ($Fe(OH)_3$) at more oxidizing environments (0.5–0.2 V) to the formation of arsenian-pyrite at increasingly reducing conditions (–0.02 to –0.2V) with the reappearance of the $Fe(OH)_3$ at more reducing conditions (<–0.17 V) as more Fe is amended into the system.

Conclusions

This study represents one of the first published field-scale studies that investigate the long-term efficiency of bioremediating arsenic-contaminated groundwater. In particular, biogeochemical reactions occurring along groundwater flow paths are documented over 1 year, including (1) the effects of changing redox conditions and water table on arsenic sequestration; (2) the effects of stimulated biogenic sulfate reduction on groundwater composition; and (3) changes in concentrations and speciation of arsenic in a contaminated aquifer. Field and laboratory data demonstrated that indigenous SRB in an arsenic-contaminated aquifer, given ample supplies of necessary electron donors (biodegradable organic carbon), electron acceptors (sulfate), and ferrous iron, were capable of anaerobically catalyzing sulfate reduction to form insoluble Fe(As)-sulfide solids. X-ray, optical, and electron microprobe analyses of the solids confirmed the precipitation of extremely small pyrite crystalline which contains 0.05–0.4 wt. % arsenic. By contrast, pure crystalline As-sulfide solids (e.g., realgar, orpiment) were not found in our Fe- and S-rich environments. It is not clear whether their growth is kinetically hindered in low-temperature environments (Lee et al. 2005) or they are outcompeted by pyrite or its precursors. More research on this is warranted. Dissolved arsenic is clearly sequestered under sulfate-reducing conditions via adsorption on the surface of iron sulfides or by co-precipitation. Arsenic may react with the reaction product H_2S to form thioarsenite aqueous complexes, thus an effective bioremediation scheme must include enough ferrous iron so that high Fe/H_2S ratios would favor the incorporation of arsenic into pyrite, instead of forming aqueous complex. In our experiment the aquifer was also amended with nutrients (N and P) to further stimulate SRB growth. It is unclear if applying additional nutrients actually aids in arsenic sequestration effectiveness because phosphorus fertilizers may cause arsenic release (Neumann et al. 2010; Aziz et al. 2017) due to ionic competition for limited mineral sorbing sites.

A similar field-scale remediation study was conducted by Pi et al. (2017) to sequester dissolved arsenic in a contaminated aquifer amended by $FeSO_4$. Their shorter (25 days) remediation process achieved significantly lower arsenic removal rates (up to 73%) with respect to ours (>90% of arsenic removal) with effective sequestration period over 6 months. The use of a mixture of organic carbon (molasses), $FeSO_4$, and fertilizer in our study better stimulates SRB and bio-mineralization than just adding $FeSO_4$, resulting in greater arsenic removal and precipitation of well-formed iron sulfide bio-nanocrystals (Figure 12). SRB metabolism was fingerprinted and verified in our study by the enrichment of heavy ^{34}S (by several per mil) in groundwater and orders of magnitude increases in SRB cells in treated groundwater. Second, in Pi et al.'s study, the fast movement of injectate in the aquifer (hundreds of meter per year) was facilitated by downgradient pumping. Transport advection processes typically dominate with respect to biogeochemical reactions in a fast-moving groundwater system. This may explain why only amorphous mineral phases or precursor mackinawite were formed over a short period of time (25 days). By contrast, advective transport is much slower in our system with groundwater flow velocity around 20 m/year. Slow injectate movement and organic carbon amendment allow biogeochemical reactions to proceed and precipitate well-formed arsenian pyrite bio-nanocrystals, which prove to be more efficient in sequestering dissolved arsenic (>90% of arsenic removal in our study) than iron sulfide precursors (only up to 73% in Pi et al. 2017).

Our study demonstrates that arsenic can be sequestered in stable biogenic pyrite in a relatively short time frame (1–2 weeks) under reducing conditions, and the sequestration can last for

at least 6 months at field scale before the arrival of untreated groundwater from upgradient. For a full-scale remediation, the biostimulation to sequester arsenic should start at positions hydrologically upgradient from the major plume (e.g., LH-2 and RA-12 at our field site, Figure 2) to allow the solutions to travel downgradient; such a scheme would prevent the re-contamination from untreated groundwater originated from up-gradient. The results also imply limited re-oxidation of sulfide solids when the amended carbon source is exhausted and when the aquifer's water table and redox condition fluctuate. Depending on site conditions, aquifers may need repeated amendment with biodegradable organic carbon to reestablish the reducing conditions that favor arsenic sequestration. This cost-effective process potentially can be modified for full-scale remediation at industrial sites.

Acknowledgments

This research has greatly benefited by assistance from our colleague Bill Hames (Auburn University) and Chris Fleischer (University of Georgia) in electron microprobe analyses, Michael Miller in SEM analysis, and Nur Ahmed in processing water samples for S isotope analysis.

Funding

This work was supported by the National Science Foundation [grant number NSF-1425004 to JS, M-KL, and AU].

References

Abraitis, P. K., R. A. D. Pattrick, and D. J. Vaughan. 2004. Variations in the compositional, textural and electrical properties of natural pyrite: a review. *Intl. J. Miner. Proc* 74(1–4):41–59.

Ahmed, K. M., P. Bhattacharya, M. A. Hasan, H. S. Akhter, S. M. M. Alam, M. A. H. Bhuyian, M. B. Imam, A. A. Khan, and O. Sracek. 2004. Arsenic enrichment in groundwater of the alluvial aquifers in Bangladesh: an overview. *Appl. Geochem*. 19(2):181–200.

Aziz, Z., B. C. Bostick, Y. Zheng, M. R. Huq, M. M. Rahman, K. M. Ahmed, and A. Van Geen. 2017. Evidence of decoupling between arsenic and phosphate in shallow groundwater of Bangladesh and potential implications. *Appl. Geochem*. 77:167–77.

Ben-Dov, E., A. Brenner, and A. Kushmaro. 2007. Quantification of sulfate reducing bacteria in industrial waste water, by real-time polymerase chain reaction (PCR) using dsrA and apsA genes. *Microbial Ecology* 54(3):439–51.

Bethke, C. M. 2008. *Geochemical and biogeochemical reaction modeling*. New York: Cambridge University Press.

Blanchard, M., M. Alfredsson, J. Brodholt, K. Wright, and C. R. A. Catlow. 2007. Arsenic incorporation into FeS_2 pyrite and its influence on dissolution: a DFT study. *Geochim. Cosmochim. Acta* 71(3):624–30.

Bostick, B. C., and S. Fendorf. 2003. Arsenic sorption on troilite (FeS) and pyrite (FeS_2). *Geochim. Cosmochim. Acta* 67(5):909–21.

Bostick, B. C., S. Fendorf, and G. E. Brown. 2005. In situ analysis of thioarsenite complexes in neutral to alkaline arsenic sulphide solutions. *Mineral Mag*. 69(05):781–95.

Bulut, G., Ü. Yenial, E. Emiroğlu, and A. A. Sirkeci. 2014. Arsenic removal from aqueous solution using pyrite. *J. Cleaner Prod*. 84:526–32.

Burton, E. D., S. G. Johnston, and B. D. Kocar. 2014. Arsenic mobility during flooding of contaminated soil: the effect of microbial sulfate reduction. *Environ. Sci. Technol*. 48(23):13660–7. –

Chapelle, F. H., and D. R. Lovley. 1992. Competitive exclusion of sulfate reduction by Fe(III) reducing bacteria: a mechanism for producing discrete zones of high-iron groundwater. *Ground Water* 30(1):29–36.

Couture, R.-M., C. Gobeil, and A. Tessier. 2010. Arsenic, iron and sulfur co-diagenesis in lake sediments. *Geochim. Cosmochim. Acta* 74(4):1238–55.

Couture, R.-M., J. Rose, N. Kumar, K. Mitchell, D. Wallschlager, and P. Van Cappellen. 2013. Sorption of arsenite, arsenate and thioarsenates to iron oxides and iron sulfides: a kinetic and spectroscopic investigation. *Environ. Sci. Technol*. 47(11):5652–9.

Deditius, A. P., M. Reich, S. E. Kesler, S. Utsunomiya, S. L. Chryssoulis, J. Walshe, and R. C. Ewing. 2014. The coupled geochemistry of Au and as in pyrite from hydrothermal ore deposits. *Geochim. Cosmochim. Acta* 140 :644–70.

Deditius, A. P., S. Utsunomiya, D. Renock, R. C. Ewing, C. V. Ramana, U. Becker, and S. E. Kesler. 2008. A proposed new type of arsenian pyrite: Composition, nanostructure and geological significance. *Geochim. Cosmochim. Acta* 72(12):2919–33.

DeSisto, S. L., H. E. Jamieson, and M. B. Parsons. 2016. Subsurface variations in arsenic mineralogy and geochemistry following long-term weathering of gold mine tailings. *Appl. Geochem*. 73:81–97.

Farquhar, M. L., J. M. Charnock, F. M. Livens, and D. J. Vaughan. 2002. Mechanisms of arsenic uptake from aqueous solution by interaction with goethite, lepidocrocite, mackinawite, and pyrite: an X-ray absorption spectroscopy study. *Environ. Sci. Technol*. 36(8):1757–62.

Gallegos, T. J., S. P. Hyun, and K. F. Hayes. 2007. Spectroscopic investigation of the uptake of arsenite from solution by synthetic mackinawite. *Environ. Sci. Technol*. 41(22):7781–6.

Gallegos, T. J., Y.-S. Han, and K. F. Hayes. 2008. Model predictions of realgar precipitation by reaction of as(III) with synthetic mackinawite under anoxic conditions *Environ. Sci. Technol.* 42(24):9338–43.

Gartman, A., and G. W. Luther. 2013. Comparison of pyrite (FeS_2) synthesis mechanisms to reproduce natural FeS_2 nanoparticles found at hydrothermal vents. *Geochim. Cosmochim. Acta* 120:447–58.

Guerin-Danan, C., C. Andrieux, and O. Szylit. 1999. Storage of intestinal bacteria in samples frozen with glycerol. *Microbial Ecol. Health Disease* 11(3):180–2.

Han, D. S., J. K. Song, B. Batchelor, and A. Abdel-Wahab. 2013. Removal of arsenite(as(III)) and arsenate(as(V)) by synthetic pyrite (FeS2): synthesis, effect of contact time, and sorption/desorption envelopes. *J. Colloid Interface Sci*. 392:311–8.

Han, Y.-S., H. Y. Jeong, A. H. Demond, and K. F. Hayes. 2011. X-ray absorption and photoelectron spectroscopic study of the association of as(III) with nanoparticulate FeS and FeS-coated sand. *Water Res*. 45(17):5727–35.

Horneman, A., A. van Geen, D. V. Kent, P. E. Mathe, Y. Zheng, R. K. Dhar, S. O'Connell, M. A. Hoque, Z. Aziz, M. Shamsudduha., et al. 2004. Decoupling of as and Fe release to Bangladesh groundwater under reducing conditions. Part I: Evidence from sediment profiles. *Geochim. Cosmochim. Acta* 68(17):3459–73.,

Huerta-Diaz, M. A., and J. W. Morse. 1992. Pyritization of trace metals in anoxic marine sediments. *Geochim. Cosmochim. Acta* 56(7):2681–702.

Jeong, H. Y., Y.-S. Han, and K. F. Hayes. 2010. X-ray absorption and x-ray photoelectron spectroscopic study of arsenic mobilization during mackinawite (FeS) oxidation. *Environ. Sci. Technol.* 44(3):955–61.

Jingtai, H., and W. S. Fyfe. 2000. Arsenic removal from water by iron-sulphide minerals. *Chin. Sci. Bull.* 45(15): 1430–4.

Keimowitz, A. R., B. J. Mailloux, P. Cole, M. Stute, H. J. Simpson, and S. N. Chillrud. 2007. Laboratory investigations of enhanced sulfate reduction as a groundwater arsenic remediation strategy. *Environ. Sci. Technol.* 41(19):6718–24.

Keimowitz, A. R., H. J. Simpson, M. Stute, S. Datta, S. N. Chillrud, J. Ross, and M. Tsang. 2005. Naturally-occurring arsenic: Mobilization at a landfill in Maine and implications for remediation. *Appl. Geochem.* 20(11): 1985–2002.

Kim, E. J., and B. Batchelor. 2009. Macroscopic and X-ray photoelectron spectroscopic investigation of interactions of arsenic with synthesized pyrite. *Environ. Sci. Technol.* 43(8):2899–904.

Kirk, M. F., E. E. Roden, L. J. Crossey, A. J. Brealey, and M. N. Spilde. 2010. Experimental analysis of arsenic precipitation during microbial sulfate and iron reduction in model aquifer sediment reactors. *Geochim. Cosmochim. Acta* 74(9):2538–55.

Kirk, M., T. Holm, J. Park, Q. Jin, R. Sanford, B. Fouke, and C. Bethke. 2004. Bacterial sulfate reduction limits natural arsenic contamination in groundwater. *Geology* 32(11):953–6.

Langner, P., C. Mikutta, and R. Kretzschmar. 2012. Arsenic sequestration by organic sulphur in peat. *Nat. Geosci.* 5(1):66–73.

Langner, P., C. Mikutta, E. Suess, M. A. Marcus, and R. Kretzschmar. 2013. Spatial distribution and speciation of arsenic in peat studied with microfocused X−ray fluorescence spectrometry and X− ray absorption spectroscopy. *Environ. Sci. Technol.* 47(17):9706–14.

Le Pape, P., M. Blanchard, J. Brest, J.-C. Boulliard, M. Ikogou, L. Stetten, S. Wang, G. Landrot, and G. Morin. 2017. Arsenic incorporation in pyrite at ambient temperature at both tetrahedral S^{-1} and octahedral Fe^{II} sites: Evidence from EXAFS-DFT analysis. *Environ. Sci. Technol.* 51(1):150–8.

Lee, M.-K., and J. A. Saunders. 2003. Effects of pH on metals precipitation and sorption: Field bioremediation and geochemical modeling approaches. *Vadose Zone J.* 2(2): 177–85.

Lee, M.-K., J. A. Saunders, R. T. Wilkin, and S. Mohammad. 2005. Geochemical modeling of arsenic speciation and mobilization: Implications for bioremediation, in advances in arsenic research: Integration of experimental and observational studies and implications for mitigation. *Am. Chem. Soc. Symp. Ser*. 915:398–413.

Lee, M.-K., J. Griffin, J. A. Saunders, Y. Wang, and J. Jean. 2007. Reactive transport of trace elements and isotopes in Alabama coastal plain aquifers. *J. Geophys. Res*. 112(G2): 2156–202.

Lee, M.-K., J. A. Saunders, and S. Nichol. 2008. Method and system for forming an in-situ groundwater filter. *US Patent* 7:341–664.

Lee, M.-K., M. Natter, J. Keevan, K. Guerra, J. A. Saunders, A. Uddin, M. Humayun, Y. Wang, and A. R. Keimowitz. 2013. Assessing effects of climate change on biogeochemical cycling of trace metals in alluvial and coastal watersheds. *Br. J. Environ. Climate Change* 3:44–66.

Lowers, H. A., G. N. Breit, A. L. Foster, J. Whitney, J. Yount, M. N. Uddin, and A. A. Muneem. 2007. Arsenic incorporation into authigenic pyrite, bengal basin sediment, Bangladesh. *Geochim. Cosmochim. Acta* 71(11): 2699–717.

Mango, H., and P. Ryan. 2015. Source of arsenic-bearing pyrite in southwestern Vermont, USA: Sulfur isotope evidence. *Sci. Tot. Environ*. 505:1331–9.

McArthur, J. M., D. M. Banerjee, K. A. Hudson-Edwards, R. Mishra, R. Purohit, P. Ravenscroft, A. Cronin, R. J. Howarth, A. Chatterjee, T. Talukder, et al. 2004. Natural organic matter in sedimentary basins and its relation to arsenic in anoxic groundwater: the example of West Bengal and its worldwide implications. *Appl. Geochem*. 19(8):1255–93.,

Meng, X., and W. Wang. 1998. *Speciation of arsenic by disposable cartridges, third international conference on arsenic exposure and health effects*. San Diego, CA, July 12–15.

Natter, M., J. Keevan, Y. Wang, A. R. Keimowitz, B. C. Okeke, A. Son, and M.-K. Lee. 2012. Level and degradation of deepwater horizon spilled oil in coastal marsh sediments and pore-Water. *Environ. Sci. Technol.* 46(11): 5744–55. –

Neumann, R. B., K. N. Ashfaque, A. B. M. Badruzzaman, A. Ali, J. K. Shoemaker, and C. F. Harvey. 2010. Anthropogenic influences on groundwater arsenic concentrations in Bangladesh. *Nat. Geosci.* 3(1):46–52.

Neumann, T., F. Scholz, M. Ostermaier, N. Rausch, and Z. Berner. 2013. Arsenic in framboidal pyrite from recent sediments of a shallow water lagoon of the Baltic Sea. *Sedimentology* 60 :1389–404.

Nordstrom, D. K. 2002. Public health. Worldwide occurrences of arsenic in ground water. *Science (New York, N.Y.)* 296(5576):2143–5.

Nordstrom, D. K., and D. G. Archer. 2003. Arsenic thermodynamic data and environmental geochemistry. In *Arsenic in ground water*. ed. A. H. Welch and K. G. Stollenwerk. 1–25. Boston: Kluwer Academic Publishers.

Nordstrom, D. K., J. Majzlan, and E. Konigsberger. 2014. Thermodynamic properties for arsenic minerals and aqueous species. *Rev. Min. Geochem.* 79(1):217–55.

O'Day, P. A. 2006. Chemistry and mineralogy of arsenic. *Elements* 2(2):77–84.

O'Day, P. A., D. Vlassopoulos, R. Root, and N. Rivera. 2004. The influence of sulfur and iron on dissolved arsenic concentrations in the shallow subsurface under changing redox conditions. *Proc. Natl. Acad. Sci.* 101(38): 13703–8.

Omoregie, E. O., R.-M. Couture, P. Van Cappellen, C. L. Corkhill, J. M. Charnock, D. A. Polya, D. Vaughan, K. Vanbroekhoven, and J. R. Lloyd. 2013. Arsenic bioremediation by biogenic iron oxides and sulfides. *Appl. Environ. Microbiol.* 79(14):4325–35.

Onstott, T. C., E. Chan, M. L. Polizzotto, J. Lanzon, and M. F. DeFlaun. 2011. Precipitation of arsenic under sulfate reducing conditions and subsequent leaching under aerobic conditions. *Appl. Geochem.* 26(3):269–85.

Pi, K., Y. Wang, X. Xie, T. Ma, Y. Liu, C. Su, Y. Zhu, and Z. Wang. 2017. Remediation of arsenic-contaminated groundwater by in-situ stimulating biogenic precipitation of iron sulfides. *Water Res.* 109:337–46.

Rieder, M., J. C. Crelling, O. Šustai, M. Drábek, Z. Weiss, and M. Klementová. 2007. Arsenic in iron disulfides in a brown coal from the North bohemian basin, Czech Republic. *Intl. J. Coal. Geol.* 71(2-3):115–21.

Rittle, K. A., J. I. Drever, and P. J. S. Colberg. 1995. Precipitation of arsenic during bacterial sulfate reduction. *Geomicrobiol. J.* 13(1):1–11.

Saunders, J. A., A. H. Hofstra, R. J. Goldfarb, and M. H. Reed. 2014. Geochemistry of Hydrothermal Gold Deposits. In *Treatise on geochemistry*. ed. H. D. Holland and K. K. Turekian. 383–424. 2nd ed. Oxford: Elsevier.

Saunders, J. A., B. E. Pivetz, N. Voorhies, and R. T. Wilkin. 2016. Potential aquifer vulnerability in regions downgradient from uranium in situ recovery (ISR) sites. *J. Environ. Manage.* 183:67–83.

Saunders, J. A. 1996. Situ bioremediation of contaminated groundwater. *US Patent* 5833855.

Saunders, J. A., M. A. Pritchett, and R. B. Cook. 1997. Geochemistry of biogenic pyrite and ferromanganese stream coatings: a bacterial connection? *Geomicrobiol. J.* 14(3):203–17.

Saunders, J. A., M.-K. Lee, L. A. Wolf, C. M. Morton, Y. Feng, I. Thomson, and S. Park. 2005. Geochemical, microbiological, and geophysical assessments of anaerobic immobilization of heavy metals. *Bioremed. J.* 9(1):33–48.

Saunders, J. A., M.-K. Lee, M. Shamsudduha, P. Dhakal, A. Uddin, M. T. Chowdury, and K. M. Ahmed. 2008. Geochemistry and mineralogy of arsenic under anaerobic conditions. *Appl. Geochem.* 23(11):3205–14.

Saunders, J. A., R. B. Cook, R. C. Thomas, and D. E. Crowe. 1996. Coprecipitation of trace metals in biogenic pyrite: Implications for enhanced intrinsic bioremediation; Bottrell, S.H. (Ed.), *Proceedings of the Fourth International Symposium on the Geochemistry of the Earth's Surface: Short Papers, International Association of Geochemists and Cosmochemists (IAGC)*, Ilkley, Yorkshire, England, July 22–28. UK: Department of Earth Sciences, University of Leeds.

Schmidt, W., and M. W. Clark. 1980. *Geology of Bay county*. Florida: Florida Geological Survey Bulletin 57, 96 p.

Shamsudduha, M., A. Uddin, J. A. Saunders, and M.-K. Lee. 2008. Quaternary stratigraphy, sediment characteristics and geochemistry of arsenic-contaminated alluvial aquifers in the ganges–brahmaputra floodplain in Central Bangladesh. *J.Contaminant. Hydrol.* 99(1-4):112–36.

Smedley, P. L., and D. G. Kinniburgh. 2002. A review of the source, behavior and distribution of arsenic in natural waters. *Appl. Geochem* 17(5):517–68.

Starnes, P. 2015. Hydrogeology and Geochemistry of Arsenic Contaminated Shallow Alluvial Aquifers in Florida and Alabama. M.S. thesis, Auburn University.

Stuckey, J. W., M. V. Schaefer, B. D. Kocar, J. Dittmar, J. Lezama Pacheco, S. G. Benner, and S. Fendorf. 2015. Peat formation concentrates arsenic within sediment deposits of the Mekong Delta. *Geochim. Cosmochim. Acta* 149 :190–205.

Sun, J., A. N. Quicksall, S. N. Chillrud, B. J. Mailloux, and B. C. Bostick. 2016. Arsenic mobilization from sediments in microcosms under sulfate reduction. *Chemosphere* 153: 254–61.

Thode, H. G., H. Kleerekoper, and E. McElcheran. 1951. *Isotope Fraction. Bacteria Reduc. Sulfate. Res. (London)*. College Park, USA: Department of Chemistry, University of Maryland. 4:581–582.

Wilkin, R. T., and R. G. Ford. 2006. Arsenic solid-phase partitioning in reducing sediments of a contaminated wetland. *Chem. Geol.* 228(1–3):156–74.

Wilkin, R. T., D. Wallschlager, and R. G. Ford. 2003. Speciation of arsenic in sulfidic waters. *Geochem. Trans.* 4(1):1–7.

Wolthers, M., I. B. Butler, and D. Rickard. 2007. Influence of arsenic on iron sulfide transformation. *Chem. Geol.* 236(3–4): 217–27.

Wolthers, M., L. Charlet, C. H. van Der Weijden, P. R. van der Linde, and D. Rickard. 2005. Arsenic mobility in the ambient sulfidic environment: Sorption of arsenic(V) and arsenic(III) onto disordered mackinawite. *Geochim. Cosmochim. Acta* 69(14):3483–92.

Yeskis, D., and B. Zavala. 2015. *Ground-Water sampling guidelines for superfund and RCRA project managers. U.S. Environmental protection agency, technical support report.* Hoboken, New Jersey, USA: Wiley Blackwell.

Zouboulis, A. I., K. A. Kydros, and K. A. Matis. 1993. Arsenic(III) and arsenic(V) removal from solutions by pyrite fines. *Separat. Sci. Tech.* 28(15–16):2449–63.